Nonlocal Ginzburg-Landau equation for cortical pattern formation

Paul C. Bressloff and Zachary P. Kilpatrick

Department of Mathematics, University of Utah, Salt Lake City, Utah 84112, USA

We show how a nonlocal version of the real Ginzburg-Landau (GL) equation arises in a large-scale recurrent network model of primary visual cortex. We treat cortex as a continuous two-dimensional sheet of cells that signal both the position and orientation of a local visual stimulus. The recurrent circuitry is decomposed into a local part, which contributes primarily to the orientation tuning properties of the cells, and a long-range part that introduces spatial correlations. We assume that (a) the local network exists in a balanced state such that it operates close to a point of instability and (b) the long-range connections are weak and scale with the bifurcation parameter of the dynamical instability generated by the local circuitry. Carrying out a perturbation expansion with respect to the long-range coupling strength then generates a nonlocal coupling term in the GL amplitude equation. We use the nonlocal GL equation to analyze how axonal propagation delays arising from the slow conduction velocities of the long-range connections affect spontaneous pattern formation.

I. INTRODUCTION

A reaction diffusion system undergoing spontaneous pattern formation can often be reduced to a (real) Ginzburg-Landau (GL) amplitude equation by carrying out a center-manifold reduction in the vicinity of a Turing instability [1,2]. The GL equation takes the form

$$\frac{\partial A}{\partial t} = \alpha A - \beta |A|^2 A + \gamma \nabla^2 A,$$

where A is the complex amplitude of the evolving pattern and α, β, γ are real coefficients. The diffusion term takes into account long-wavelength modulations of the spatially periodic (roll) pattern arising from excitation of a band of spatial frequencies in a neighborhood of the critical Turing frequency. (In the case of two spatial dimensions, there must be some form of spatial anisotropy in the system otherwise one obtains the Newell-Whitehead-Segel amplitude equation [3,4]). The GL equation provides qualitative insights into some universal features of the dynamics of pattern forming reaction diffusion systems [5].

The complex Ginzburg Landau (CGL) equation (complex coefficients α, β, γ) plays an analogous role in the case of oscillatory reaction diffusion systems that are close to a supercritical Hopf bifurcation [6]. Recently, a modified version of the CGL equation has been derived in which diffusive coupling is replaced by nonlocal coupling [7]. At first sight this appears counterintuitive, since even if the original system consisted of oscillators with nonlocal coupling, the CGL equation describes patterns whose characteristic wavelength becomes considerably longer than the effective range of coupling as the bifurcation point is approached. However, suppose that a system of chemical components constitute local (nondiffusing) oscillators that are coupled via an additional chemical component that diffuses freely. If the strength of diffusive coupling is sufficiently weak so that it scales with the associated Hopf bifurcation parameter, then the resulting CGL amplitude equation has nonlocal coupling. One of the interesting features of the nonlocal CGL equation is that it

exhibits new types of instability not found in the standard CGL equation [7–9].

In this paper we show how a nonlocal version of the real GL equation arises in a large-scale recurrent network model of primary visual cortex (V1). Following Bressloff *et al.* [10–12], we treat cortex as a continuous two-dimensional sheet of cells that signal both the position and orientation of a local visual stimulus. The recurrent circuitry is decomposed into a local part, which contributes primarily to the orientation tuning properties of the cells, and a long-range part that introduces spatial correlations. We also incorporate axonal propagation delays into the long-range connections in order to take into account the fact that they have slow conduction velocities. In previous work we used symmetric bifurcation theory and perturbation methods to derive a set of amplitude equations for the selection and stability of spatially periodic cortical patterns in the absence of delays; these amplitude equations took the form of a system of coupled ODEs [10–12]. We thus showed how spontaneous cortical activity patterns underlying common visual hallucinations can be accounted for in terms of certain symmetry properties of the long-range recurrent connections, specifically, that they are invariant under the so-called shift-twist action of the Euclidean group. The resulting group representation is twisted due to an anisotropy in the long-range connections, which tends to favor directions that are correlated with the orientation preferences of the interacting cells. Here we develop an alternative perturbation scheme for analyzing cortical pattern formation based on a nonlocal GL equation, see also Ref. [14], and use this to explore the effects of axonal propagation delays on spontaneous pattern formation. The nonlocal GL equation is derived by assuming that the long-range connections are weak and scale with the bifurcation parameter of a dynamical instability that is generated by the local circuitry. One useful feature of the nonlocal GL equation is that it explicitly separates out the local and long-range contributions to cortical dynamics, thus simplifying the analysis of spatiotemporal patterns. It also provides a continuum modeling framework for studying how long-range connections modulate the effects of external visual

stimuli along similar lines to the spatially discrete model of Bressloff and Cowan [13].

The structure of the paper is as follows. In Sec. II we introduce our cortical model. In Sec. III we derive the non-local GL equation by carrying out a perturbation expansion with respect to a coupling parameter that determines the strength of the long-range connections. In Sec. IV we use the nonlocal GL equation to analyze the effects of axonal propagation delays on spontaneous pattern formation. First, we show how in the absence of axonal delays, the nonlocal GL equation undergoes a Turing instability that breaks the underlying Euclidean shift-twist symmetry, leading to spatially periodic patterns consistent with our previous work. The Turing instability is generated by purely inhibitory long-range connections rather than by the standard Mexican hat weight distribution, reflecting the existence of a gap. We then show that sufficiently long axonal delays can lead to a bulk Hopf instability rather than a Turing instability. Note that in this paper we consider nonlocal synaptic coupling within the context of large-scale rate based models of cortex. This should be contrasted with models that study the effects of nonlocal synaptic coupling between individual neuronal oscillators sitting close to a subcritical or supercritical Hopf bifurcation [15–17]. Here convolution terms representing the synaptic coupling are incorporated into the normal forms of the individual oscillators.

II. A CONTINUUM MODEL OF V1 AND ITS INTRINSIC CIRCUITRY

A. Functional anatomy of V1

Primary visual cortex (V1) is the first cortical area to receive visual information transmitted by ganglion cells of the retina via the lateral geniculate nucleus (LGN) of the thalmus to the back of the brain. A fundamental property of the functional architecture of V1 is an orderly retinotopic mapping of the visual field onto the surface of cortex, with the left and right halves of visual field mapped onto the right and left cortices, respectively. Superimposed upon the retinotopic map are a number of additional feature maps reflecting the fact that neurons respond preferentially to stimuli with particular features [18,19]. For example, most cortical cells signal the local orientation of a contrast edge or bar—they are tuned to a particular local orientation [20]. Other possible stimulus preferences include a left/right eye preference known as ocular dominance, spatial frequency and color. In recent years considerable information about the two-dimensional [21] distribution of both orientation preference and ocular dominance across the cortical surface has been obtained using optical imaging techniques [22–24]. The basic topography revealed by these methods suggests V1 has an approximately periodic microstructure (with period around 1 mm in cats and primates) so that cortex can be partitioned into a set of local functional modules or hypercolumns [18,25,26], each of which carries out some form of local image processing.

The existence of a set of feature preference maps has implications for the functional anatomy of V1. There appear to be at least two functional circuits acting on different
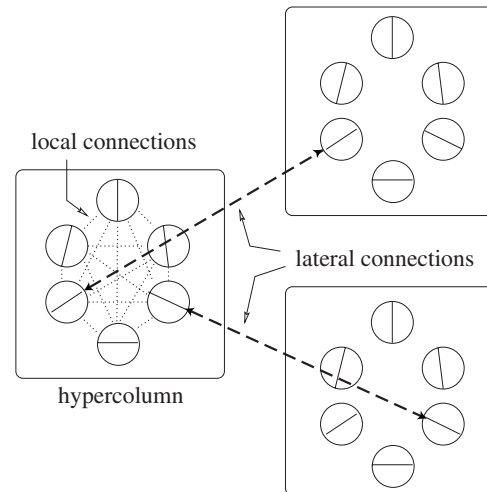

FIG. 1. Schematic illustration of isotropic local connections within a hypercolumn and anisotropic lateral connections between hypercolumns. Each disc represents a local population of cells whose common orientation preference is indicated by the orientation of a diagonal bar.

length scales within a cortical layer. There is a local circuit operating at subhypercolumn dimensions in which cells make connections with most of their neighbors in a roughly isotropic fashion [27,28]. It has been suggested that such circuitry provides a substrate for the recurrent amplification and sharpening of the tuned response of cells to local visual stimuli [29,30]. The other circuit operates between hypercolumns and is mediated by so-called patchy horizontal connections [31,32]. Optical imaging combined with cell labeling techniques have generated considerable information concerning the pattern of these connections in superficial layers of V1 [33–35]. In particular, one finds that the patchy horizontal connections tend to link cells with similar feature preferences. Moreover, in tree shrew and cat there is a pronounced anisotropy in the distribution of patchy connections, with differing iso-orientation patches preferentially connecting to neighboring patches in such a way as to form continuous contours following the topography of the retinocortical map [35], see Fig. 1. That is, the major axis of the horizontal connections tends to run parallel to the visuotopic axis of the connected cells' common orientation preference. There is also a clear anisotropy in the patchy connections of owl [36] and macaque [37,38] monkeys. However, in these cases most of the anisotropy can be accounted for by the fact that V1 is expanded in the direction orthogonal to ocular dominance columns. Interestingly, the recently observed patchy feedback connections from extrastriate areas in primates tend to be more strongly anisotropic [37] and to exhibit similar forms of anisotropy as previously found for horizontal connections in tree shrew [39]. Stimulation of a hypercolumn via lateral connections modulates rather than initiates spiking activity [41], suggesting that the long-range interactions provide local cortical processes with contextual information about the global nature of stimuli. As a consequence the horizontal connections have been invoked to explain a wide variety of context-dependent visual processing phenomena [42–44].

B. The model

Suppose that cortex is treated as an unbounded two-dimensional sheet and let a denote the population activity of a local pool of neurons in a given volume element of a slab of neural tissue located at $\mathbf{r} \in \mathbf{R}^2$. The neural field a is taken to evolve according to the Wilson-Cowan equation [45,46]

$$\tau_m \frac{\partial a(\mathbf{r},t)}{\partial t} = -a(\mathbf{r},t) + \int_{\mathbf{R}^2} w(\mathbf{r}|\mathbf{r}')f[a(\mathbf{r}',t)]d\mathbf{r}' + h(\mathbf{r},t),$$

(2.1)

where $w(\mathbf{r}|\mathbf{r}')$ is the weight per unit volume of all synapses at $\mathbf{r}$ from neurons at $\mathbf{r}'$, h is the feedforward (excitatory) input from the LGN or other cortical layers, and τ_m is a synaptic time constant. (We fix the units of time by setting $\tau_m=1$; for fast synapses the time constant can be around 5 ms.) The nonlinearity f is taken to be a smooth output function of the form

$$f(a) = \frac{f_0}{1 + e^{-\eta(a-\kappa)}},$$

(2.2)

where f_0 is the maximum firing rate that is taken to be unity for the given units of time, η determines the slope or gain of the input-output characteristics of the population, and κ is a threshold. One common assumption regarding the structure of the synaptic connections w is that they depend only on cortical separation $|\mathbf{r}-\mathbf{r}'|$ so that $w(\mathbf{r}|\mathbf{r}') \to w(|\mathbf{r}-\mathbf{r}'|)$. The weight distribution is then invariant under the action of the Euclidean group $\mathbf{E}(2)$ of rigid motions in the plane, that is,

$$\gamma w(\mathbf{r}|\mathbf{r}') = w(\gamma^{-1} \cdot \mathbf{r}|\gamma^{-1} \cdot \mathbf{r}') = w(\mathbf{r}|\mathbf{r}')$$

(2.3)

for all $\gamma \in \mathbf{E}(2)$. The Euclidean group is composed of the (semidirect) product of $\mathbf{O}(2)$, the group of planar rotations $\mathbf{r} \to R_\varphi \mathbf{r}$ and reflections $(x,y) \to (x,-y)$, with $\mathbf{R}^2$, the group of planar translations $\mathbf{r} \to \mathbf{r}+\mathbf{s}$. Here

$$R_\varphi = \begin{pmatrix} \cos\varphi & -\sin\varphi \\ \sin\varphi & \cos\varphi \end{pmatrix}, \quad \varphi \in [0,2\pi).$$

(2.4)

Euclidean symmetry considerably simplifies the analysis of spontaneous pattern formation and traveling waves in cortical models (see the reviews [47,48]). However, as we have emphasized elsewhere [49,50], planar Euclidean symmetry no longer holds when the structure of patchy horizontal connections is taken into account. Unfortunately, incorporating this structure into the weight distribution w is nontrivial, since it requires the specification of a set of feature maps that describe the variation of stimulus feature preferences as a function of cortical position $\mathbf{r}$. One way to avoid this problem is to introduce a different coordinate system for labeling cortical cells based on a spatial coarse graining of $\mathbf{r}$. One approach is to partition cortex into a set of hypercolumns with $\mathbf{r}$ specifying the location of an individual hypercolumn within the cortical sheet, leading to the so-called coupled hypercolumn model of cortex [10,13], see also Fig. 1. Neurons are now labeled by the independent set $(\mathbf{r},\mathcal{F})$ where $\mathcal{F}$ specifies the set of feature preferences of a cell within a given hypercolumn. One of the potential difficulties in identifying $\mathbf{r}$ as a hypercolumn label is that the level of spatial coarse graining is rather severe. Moreover, there is not a unique way of partitioning cortex into a set of functional hypercolumns, that is, the hypercolumn effectively corresponds to a length scale rather than a well-defined physical domain.

Here we consider a modified labeling scheme that avoids the above difficulties by explicitly taking into account the fact that each cortical neuron responds to light stimuli in a restricted region of the visual field called its classical receptive field (RF). Patterns of illumination outside the RF of a given neuron cannot generate a response directly, although they can significantly modulate responses to stimuli within the RF via patchy horizontal and feedback connections [44,51]. A visual stimulus is typically described in terms of a function $s(X,Y,t)$ that is proportional to the difference between the luminance at point (X,Y) in the visual field at time t and the average or background level of luminance (since the visual system adapts to the background illumination). Often s is divided by the background luminance level, making it a dimensionless quantity called the contrast. Assuming a linear relationship between the feedforward input $h(\mathbf{r},t)$ to a neuron at $\mathbf{r}$ and the stimulus s, we can take

$$h(\mathbf{r},t) = \int_0^\infty \int_{\mathbf{R}^2} D_{\mathbf{r}}[X - \bar{X}(\mathbf{r}), Y - \bar{Y}(\mathbf{r}), \tau]$$
$$\times s(X,Y,t-\tau)dXdYd\tau,$$

(2.5)

where $D_{\mathbf{r}}$ is the space-time RF profile of the neuron and $[\bar{X}(\mathbf{r}), \bar{Y}(\mathbf{r})]$ is the RF center in visual coordinates. (Neurons that carry out a linear RF summation are termed simple cells, whereas neurons with nonlinear RF properties are called complex cells [52].) The RF profile $D_{\mathbf{r}}$ depends on the various stimulus feature preferences $\mathcal{F}(\mathbf{r})$ of the neuron at $\mathbf{r}$ including its orientation preference $\theta(\mathbf{r})$. Hence, the variation of the input $h(\mathbf{r},t)$ with cortical position $\mathbf{r}$ depends on the distribution of RF centers $[\bar{X}(\mathbf{r}), \bar{Y}(\mathbf{r})]$ and the associated feature preference maps $\mathcal{F}(\mathbf{r})$. It follows that the location of the RF center is another "feature" of a cortical cell. It is convenient to represent the RF center in cortical coordinates, rather than visual coordinates. Therefore, we introduce an invertible retinocortical map Φ, which specifies how a visual image maps to a corresponding activity pattern in V1 [53]; it can be shown that in appropriate coordinates Φ is well approximated by a complex logarithm [54]. We then set $\bar{\mathbf{r}} = \Phi(\bar{X}, \bar{Y})$ and relabel cortical cells according to the set $(\bar{\mathbf{r}}, \mathcal{F})$ with $\bar{\mathbf{r}}$ and $\mathcal{F}$ treated as independent variables. Thus, one can view the coordinate $\bar{\mathbf{r}}$ as a coarse-grained version of cortical position $\mathbf{r}$ that is nevertheless defined on a finer spatial scale than a hypercolumn label, commensurate with spatial visual acuity. Neurons at different spatial locations within the same hypercolumn tend to have similar RF centers, whereas there is a systematic shift in the RF center as one moves across neighboring hypercolumns. Implicit in our labeling scheme are the assumptions that the various feature maps are independent or separable, and that the retinotopic map is smooth. These assumptions are consistent with a number of experimental studies [55–57], although nonseparability has also been observed [58].

Having motivated the new labeling scheme, we rewrite $\bar{\mathbf{r}}$ as $\mathbf{r}$ with the understanding that $\mathbf{r}$ now represents the RF center in cortical coordinates. For simplicity, we only consider orientation preference by setting $\mathcal{F} = \theta \in [0, \pi)$; this will be sufficient to incorporate the patchy, anisotropic nature of long-range connections. Let $a(\mathbf{r}, \theta, t)$ denote the activity of the population with cortical label $(\mathbf{r}, \theta)$, and consider the evolution equation

$$\frac{\partial a(\mathbf{r}, \theta, t)}{\partial t} = -a(\mathbf{r}, \theta, t) + h(\mathbf{r}, \theta, t)$$

$$+ \int_{\mathbf{R}^2} \int_0^\pi w(\mathbf{r}, \theta | \mathbf{r}', \theta') f[a(\mathbf{r}', \theta', t)] \frac{d\theta'}{\pi} d\mathbf{r}'.$$

$$(2.6)$$

Note that there is no simple coordinate transformation relating Eqs. (2.6) and (2.1) and their corresponding weight kernels w. Moreover, both models ignore details at sufficiently small length scales by treating the cortex as a continuum. The planar model neglects features at the length scale of individual neurons, whereas the coupled hypercolumn model neglects features at length scales smaller than those corresponding to normal visual acuity. The continuum approximation is valid provided that solutions to the model equations involve coherent structures whose length scales are at least an order of magnitude greater than the fundamental length scale.

Following our discussion regarding the intrinsic circuitry of V1, we decompose the weight distribution w of Eq. (2.6) into distinct local and a long-range contributions according to [59]

$$w(\mathbf{r}, \theta | \mathbf{r}', \theta') = w(\theta - \theta') H(d_0 - |\mathbf{r} - \mathbf{r}'|)/(\pi d_0^2)$$

$$+ \beta w_{\text{hoz}}(\mathbf{r}, \theta | \mathbf{r}', \theta') H(|\mathbf{r} - \mathbf{r}'| - d_1),$$

$$(2.7)$$

where $d_0 \ll d_1$ with d_1 denoting the typical spacing (of around 0.3–1 mm) between neighboring hypercolumns, H is the Heaviside function, and β is a small coupling parameter that incorporates the finding that the horizontal connections tend to be modulatory in nature [40,41]. In order to specify the size of β, we normalize the total weight of both the local and long-range connections to be unity, that is, we set $\int_0^\pi w(\theta) d\theta / \pi = 1$ and

$$\int_{\mathbf{R}^2} \int_0^\pi w_{\text{hoz}}(\mathbf{r}, \theta | \mathbf{r}', \theta') \frac{d\theta'}{\pi} d\mathbf{r}' = 1 \qquad (2.8)$$

for all $\mathbf{r}, \theta$. We then set $\beta = \varepsilon \beta_0$ where ε is a small dimensionless parameter with $\varepsilon \ll 1$, and $\beta_0 = \pm 1$ specifies whether the horizontal connections have a net excitatory or inhibitory effect on the local circuits. Although the horizontal connections are excitatory, since they are mediated by long axonal projections of pyramidal cells [47,26], 20% of the connections in layers II and III of V1 end on inhibitory interneurons, so the overall action of the horizontal connections can become inhibitory, especially at high levels of activity [40].

We assume that cells with sufficiently similar RF centers ($|\mathbf{r} - \mathbf{r}'| < d_0$) interact according to a local weight distribution

$w(\theta - \theta')$ that depends on the relative orientation preference of interacting cells. On the other hand, cells with sufficiently well separated RF centers ($|\mathbf{r} - \mathbf{r}'| > d_1$) interact according to the rules of long-range horizontal connections

$$w_{\text{hoz}}(\mathbf{r}, \theta | \mathbf{r}', \theta') = \mathcal{G}(|\mathbf{r} - \mathbf{r}'|) w^\Delta(\theta - \theta) \mathcal{P}\{\arg(\mathbf{r} - \mathbf{r}')$$

$$- [\theta + \theta']/2\}.$$

$$(2.9)$$

The first factor $\mathcal{G}$ incorporates the observation that the density of patches tends to decrease monotonically with cortical separation. For concreteness, we take $\mathcal{G}(s)$ to be a Gaussian

$$\mathcal{G}(s) = \mathcal{N} e^{-(s - d_1)^2 / 2\xi^2}, \quad s \geq d_1, \qquad (2.10)$$

where ξ determines the range of the horizontal connections and $\mathcal{N}$ is a normalization factor such that $\int_{d_1}^\infty s \mathcal{G}(s) ds = 1$. The horizontal connections have a typical range of 2–6 mm, although the effective range would be considerably longer if feedback connections were taken into account [38]. (We fix the units of length by setting $\xi = 1$.) The second factor in Eq. (2.9) w^Δ ensures that the long-range connections link cells with similar orientation preferences, and is taken to be a positive, narrowly tuned distribution with $w^\Delta(\theta) = 0$ for all $|\theta| > \theta_c$ and $\theta_c \ll \pi/2$. The final factor $\mathcal{P}$ incorporates the anisotropic nature of the patchy connections, namely, that the common orientation preference of interacting populations [taken for mathematical convenience to be the arithmetic mean $(\theta + \theta')/2$] is correlated with the direction $\arg(\mathbf{r} - \mathbf{r}')$ in the plane linking these cell populations. One possible choice for $\mathcal{P}$ is

$$\mathcal{P}(\psi) = \frac{1}{4\eta} [H(\eta - |\psi|) + H(\eta - |\psi - \pi|)], \qquad (2.11)$$

where η is a measure of the degree of spread or anisotropy in the horizontal connections. The functions $w(\theta)$ and $w^\Delta(\theta)$ are both assumed to be even, π-periodic functions of θ, with corresponding Fourier expansions

$$w(\theta) = W_0 + 2 \sum_{n \geq 1} W_n \cos 2n\theta,$$

$$w^\Delta(\theta) = W_0^\Delta + 2 \sum_{n \geq 1} W_n^\Delta \cos 2n\theta. \qquad (2.12)$$

The large-scale cortical model given by Eqs. (2.6), (2.7), and (2.9) does not take into account one important aspect of the orientation preference map, namely, the existence of orientation singularities or pinwheels [23,24]. That is, orientation domains tend to be organized radially around pinwheel centers at which the representations of all orientations converge. Intracellular recordings suggest that the spike response of individual neurons at pinwheel centers are sharply tuned for orientation, even though their subthreshold response is broadly tuned, whereas cells away from pinwheels have sharply tuned super- and subthreshold responses [60,61] (but see Ref. [62]). Hence, it is possible that the role of local circuitry in generating the tuned response to oriented stimuli depends on cortical location [28]. The heterogeneous

nature of the orientation preference map due to pinwheels has been incorporated into a detailed computational model of several hypercolumns [52,63]. However, it is difficult to extend such a model to take into account the large-scale structure of cortex without carrying out some form of spatial coarse graining [64]. An alternative approach to modeling pinwheels is to start with a coarse-grained approach that considers the tuning properties of local populations of cells rather than of individual neurons. From this perspective, the high degree of scatter of orientation preferences around a pinwheel center means that the corresponding population activity is poorly tuned for orientation preference. This can be incorporated into a generalization of the model presented here, in which $\mathcal{F}$ includes both the orientation and the spatial frequency maps [65]. Now the local weight distribution is expanded in terms of spherical harmonics rather than simple Fourier harmonics. Interestingly, a recent topological analysis of population activity in V1 indicates that both spontaneous activity and activity evoked by natural images is consistent with the topology of a two sphere [66].

C. Symmetries of model

If there is no orientation-dependent anisotropy ($\mathcal{P} \equiv 1$), then the weight distribution (2.7) is invariant with respect to the symmetry group $\mathbf{E}(2) \times \mathbf{O}(2)$, where $\mathbf{O}(2)$ is the group of rotations and reflections on the ring S^1 and $\mathbf{E}(2)$ is the Euclidean group acting on $\mathbf{R}^2$. The associated group action is

$$\zeta(\mathbf{r}, \theta) = (\zeta \mathbf{r}, \theta), \quad \zeta \in \mathbf{E}(2),$$

$$\xi(\mathbf{r}, \theta) = (\mathbf{r}, \theta + \xi),$$

$$\kappa(\mathbf{r}, \theta) = (\mathbf{r}, -\theta). \tag{2.13}$$

Invariance of the weight distribution can be expressed as

$$\gamma w(\mathbf{r}, \theta | \mathbf{r}', \theta) = w[\gamma^{-1}(\mathbf{r}, \theta) | \gamma^{-1}(\mathbf{r}', \theta')] = w(\mathbf{r}, \theta | \mathbf{r}', \theta') \tag{2.14}$$

for all $\gamma \in \Gamma$ where $\Gamma = \mathbf{E}(2) \times \mathbf{O}(2)$. Anisotropy reduces the symmetry group Γ to $\mathbf{E}(2)$ with the following shift-twist action on $\mathbf{R}^2 \times S^1$ [10,11]:

$$\mathbf{s}(\mathbf{r}, \theta) = (\mathbf{r} + \mathbf{s}, \theta),$$

$$\xi(\mathbf{r}, \theta) = (R_\xi \mathbf{r}, \theta + \xi),$$

$$\kappa(\mathbf{r}, \theta) = (R_\kappa \mathbf{r}, -\theta), \tag{2.15}$$

where R_ξ denotes the planar rotation through an angle ξ and R_κ denotes the reflection $(x_1, x_2) \mapsto (x_1, -x_2)$. It can be seen that the discrete rotation operation comprises a translation or shift of the orientation preference label θ to $\theta + \xi$, together with a rotation or twist of the position vector $\mathbf{r}$ by the angle ξ. It is instructive to establish explicitly the invariance of anisotropic long-range connections under shift-twist symmetry. Translation invariance of w_{hoz} in Eq. (2.9) follows

immediately from the spatial homogeneity of the interactions, which implies that

$$w_{\text{hoz}}(\mathbf{r} - \mathbf{s}, \theta | \mathbf{r}' - \mathbf{s}, \theta') = w_{\text{hoz}}(\mathbf{r}, \theta | \mathbf{r}', \theta').$$

Invariance with respect to a rotation by ξ follows from

$$
\begin{aligned}
w_{\text{hoz}}&(R_{-\xi}\mathbf{r}, \theta - \xi | R_{-\xi}\mathbf{r}', \theta' - \xi) \\
&= \mathcal{G}[|R_{-\xi}(\mathbf{r} - \mathbf{r}')|]\mathcal{P}\{\arg[R_{-\xi}(\mathbf{r} - \mathbf{r}')] \\
&\quad - (\theta + \theta')/2 + \xi\}w^\Delta(\theta - \xi - \theta' + \xi), \\
&= \mathcal{G}(|\mathbf{r} - \mathbf{r}'|)\mathcal{P}[\arg(\mathbf{r} - \mathbf{r}') - (\theta + \theta')/2]w^\Delta(\theta - \theta') \\
&= w_{\text{hoz}}(\mathbf{r}, \theta | \mathbf{r}', \theta').
\end{aligned}
$$

We have used the conditions $|R_\xi \mathbf{r}| = |\mathbf{r}|$ and $\arg(R_{-\xi}\mathbf{r}) = \arg(\mathbf{r}) - \xi$. Finally, invariance under a reflection κ about the x axis holds since

$$
\begin{aligned}
w_{\text{hoz}}(\kappa\mathbf{r}, -\theta | \kappa\mathbf{r}', -\theta') &= \mathcal{G}[|\kappa(\mathbf{r} - \mathbf{r}')|]\mathcal{P}\{\arg[\kappa(\mathbf{r} - \mathbf{r}')] \\
&\quad + (\theta + \theta')/2\}w^\Delta(-\theta + \theta'), \\
&= \mathcal{G}(|\mathbf{r} - \mathbf{r}'|)\mathcal{P}[-\arg(\mathbf{r} - \mathbf{r}') \\
&\quad + (\theta + \theta')/2]w^\Delta(\theta - \theta'), \\
&= w_{\text{hoz}}(\mathbf{r}, \theta | \mathbf{r}', \theta').
\end{aligned}
$$

We have used the conditions $\arg(\kappa\mathbf{r}) = -\arg(\mathbf{r})$, $w^\Delta(-\theta) = w^\Delta(\theta)$, and $\mathcal{P}(-\psi) = \mathcal{P}(\psi)$. The fact that the weight distribution is invariant with respect to this shift-twist action has important consequences for the global dynamics of V1 in the presence of anisotropic horizontal connections [10,11].

D. Axonal propagation delays

Another important property of long-range horizontal connections is that the speed of action potential propagation along the axons of these connections is relatively slow. Typical speeds of 0.2–0.4 m/s have been measured electrically in both cat V1 [40] and primate V1 [67]; such speeds are at least an order of magnitude slower than those found for feedforward and feedback connections [67]. (In terms of the given space and time units with $\tau_m = 5$ ms, $\xi = 5$ mm, and $v = 0.2$ ms^{-1}, we have the dimensionless quantity $v\tau_m/\xi = 0.2$.) A number of theoretical studies have incorporated finite propagation speeds in neural field models [68–76], and shown that for sufficiently small propagation speeds v axonal delays can lead to oscillatory patterns. In contrast to these studies, we explicitly distinguish between local and long-range horizontal connections and assume that axonal propagation delays only occur in the latter. That is, we incorporate axonal delays into our cortical model given by Eqs. (2.6) and (2.7) according to

$$\frac{\partial a(\mathbf{r},\theta,t)}{\partial t} = -a(\mathbf{r},\theta,t) + h(\mathbf{r},\theta,t) + \frac{1}{\pi d_0^2}\int_{\mathbf{R}^2}\int_0^\pi w(\theta-\theta')H(d_0-|\mathbf{r}-\mathbf{r}'|)f[a(\mathbf{r}',\theta',t)]\frac{d\theta'}{\pi}d\mathbf{r}'$$

$$+ \beta\int_{\mathbf{R}^2}\int_0^\pi w_{\text{hoz}}(\mathbf{r},\theta|\mathbf{r}',\theta')H(|\mathbf{r}-\mathbf{r}'|-d_1)f[a(\mathbf{r}',\theta',t-|\mathbf{r}-\mathbf{r}'|/v)]\frac{d\theta'}{\pi}d\mathbf{r}'. \quad (2.16)$$

Note that inclusion of axonal delays preserves the Euclidean shift-twist symmetry of our model.

III. DERIVATION OF NONLOCAL GINZBURG-LANDAU EQUATION

In previous work we showed how a uniform solution of Eq. (2.6) for a constant input h can undergo a Turing-like instability that spontaneously breaks the underlying Euclidean shift-twist symmetry, leading to the formation of spatially periodic patterns. We used symmetric bifurcation theory to analyze the selection and stability of the resulting patterns, and by mapping the patterns to visual coordinates via the inverse retinotopic map, we showed how the patterns reproduce a variety of common geometric visual hallucinations [10–12]. In particular, we established that the original Ermentrout-Cowan theory of visual hallucinations [77] can be extended to the case of contoured images by the inclusion of the orientation preference label θ into the cortical model (2.6). Here we follow a different approach by first considering instabilities of the uniform state in the absence of horizontal connections. We then perform a perturbation expansion with respect to the long-range coupling parameter ε in order to derive an amplitude equation for the growth of cortical activity patterns. The amplitude equation takes the form of a nonlocal Ginzburg-Landau (GL) equation whose integration kernel is determined by the horizontal connections.

In the case of zero horizontal connections ($\varepsilon=0$) and constant inputs [$h(\theta,\mathbf{r},t)=\bar{h}$], Eq. (2.6) reduces to

$$\frac{\partial a(\mathbf{r},\theta,t)}{\partial t} = -a(\mathbf{r},\theta,t) + \bar{h} + \int_{\mathbf{R}^2}\int_0^\pi \Delta(|\mathbf{r}-\mathbf{r}'|)$$

$$\times w(\theta-\theta')f(a(\mathbf{r}',\theta',t))\frac{d\theta'}{\pi}d\mathbf{r}', \quad (3.1)$$

where $\Delta(s)=H(d_0-s)/(\pi d_0^2)$. In the case of a constant input there exists at least one uniform equilibrium solution of Eq. (3.1), which satisfies the algebraic equation

$$\bar{a} = W_0 f(\bar{a}) + \bar{h} \quad (3.2)$$

with $W_0=\int_0^\pi w(\theta)d\theta/\pi=1$. If $\bar{h}$ is sufficiently small relative to the threshold κ of the neurons then the equilibrium is unique and stable. Under the change of coordinates $a\rightarrow a-\bar{h}$, it can be seen that the effect of $\bar{h}$ is to shift the threshold by the amount $-\bar{h}$. Thus, there are two ways to increase the excitability of the network and thus destabilize the fixed point: either by increasing the external input $\bar{h}$ or reducing

the threshold κ. The latter can occur through the action of drugs on certain brain stem nuclei, which provides a mechanism for generating geometric visual hallucinations [10–12,77].

The stability of the fixed point can be determined by setting $a(\mathbf{r},\theta,t)=\bar{a}+a(\mathbf{r},\theta)e^{\lambda t}$ and linearizing about $\bar{a}$. This leads to the linear evolution equation

$$\lambda a(\mathbf{r},\theta) = -a(\mathbf{r},\theta) + \mu\int_{\mathbf{R}^2}\int_0^\pi \Delta(|\mathbf{r}-\mathbf{r}'|)$$

$$\times w(\theta-\theta')a(\mathbf{r}',\theta')\frac{d\theta'}{\pi}d\mathbf{r}', \quad (3.3)$$

where $\mu=f'(\bar{a})$. This has eigensolutions of the form $a(\mathbf{r},\theta)=e^{\lambda t}e^{i\mathbf{k}\cdot\mathbf{r}}e^{2in\theta}$ with λ satisfying the dispersion relation

$$\lambda = \lambda_n(k) \equiv -1 + \mu\tilde{\Delta}(k)W(n), \quad n\in\mathbf{Z}, \quad (3.4)$$

where $k=|\mathbf{k}|$,

$$\tilde{\Delta}(k) = \int_{\mathbf{R}^2}e^{i\mathbf{k}\cdot\mathbf{r}}\Delta(|\mathbf{r}|)d\mathbf{r} = \frac{2}{d_0^2}\int_0^{d_0}rJ_0(kr)dr \quad (3.5)$$

and J_0 is the zeroth order Bessel function. It follows that for sufficiently small μ, corresponding to a low activity state $\lambda_n(k)<0$ for all n,k so the fixed point is stable. However, as μ is increased beyond a critical value μ_c the fixed point becomes unstable due to excitation of the eigensolutions associated with the largest Fourier components. Suppose that $W_M=\max_m\{W_m\}$. Since $\max_k\{\tilde{\Delta}(k)\}=\tilde{\Delta}(0)=1$, it follows that the fixed point will become unstable at $\mu_c=1/W_M$ leading to the growth of a pattern of the form

$$a(\mathbf{r},\theta) = z(\mathbf{r})e^{2iM\theta} + \bar{z}(\mathbf{r})e^{-2iM\theta} = A(\mathbf{r})\cos\{2M[\theta-\theta_0(\mathbf{r})]\} \quad (3.6)$$

with complex amplitude $z=Ae^{-2i\theta_0}$. In the absence of horizontal connections we expect the resulting pattern to be approximately $\mathbf{r}$ independent due to the dominance of the $k=0$ mode, that is, orientation tuning will be coherent across cortex with maximal responses at $\theta=\theta_0+\pi/M$. In this paper, we will assume that the dominant discrete mode is $M=1$ so that orientation tuning curves have a single maximum at $\theta=\theta_0$. The peak θ_0 is arbitrary and depends only on random initial conditions, reflecting the spontaneous breaking of the underlying $\mathbf{O}(2)$ symmetry. Since the dominant Fourier component is W_1, the local distribution $w(\theta)$ is excitatory (inhibitory) for neurons with sufficiently similar (dissimilar) orientation preferences. (This is analogous to the Wilson-Cowan "Mexican Hat" function [46].) If the local level of inhibition

were reduced so that W_n were a monotonically decreasing function of $|n|$ with $M=0$, then the homogeneous fixed point would undergo a bulk instability at $\mu_c=1/W_0$ and there would be no orientation tuning.

Let us now consider the effect of perturbatively switching on the horizontal connections ($\varepsilon > 0$) and that the system operates within $O(\varepsilon)$ of the bifurcation point for excitation of the $M=1$ eigenmode in the absence of horizontal connections, see Eq. (3.6), that is, $\mu=\mu_c(1+\varepsilon\Delta\mu)$ with μ_c the critical point. (This is analogous to assuming that weak diffusive coupling scales with the bifurcation parameter in oscillatory reaction diffusion systems [7].) For sufficiently small d_0 there will be a wide band of excited modes beyond the critical point due to the condition $\widetilde{\Delta}(k)\approx 1$ for $k<1/d_0$. We assume that the horizontal connections select a particular wavelength within this band of excited modes that is of order ξ, and this determines the coherence length of the resulting spontaneous activity patterns. Assuming that $\xi\gg d_0$, it follows that the length-scale d_0 does not play a significant role and we can take the limit $d_0\to 0$ in Eq. (2.16) so that $\Delta(s)\to\delta(s)$. We then carry out a perturbation expansion of Eq. (2.16) in powers of the small coupling parameter ε. For ease of notation, we will first carry out the derivation in the absence of axonal delays by taking $v\to\infty$ in Eq. (2.16). We will then show how to extend the analysis to incorporate delays.

First, perform a Taylor expansion of Eq. (2.16) about the fixed point $\bar{a}$ by setting $b(\mathbf{r},\theta,t)=a(\mathbf{r},\theta,t)-\bar{a}$ and taking $d_0\to 0$, $v\to\infty$:

$$\frac{\partial b}{\partial t}=-b+w*[\mu b+\gamma b^2+\gamma' b^3+\cdots]+\varepsilon\beta_0 w_{\text{hoz}}\circ([f(\bar{a})$$

$$+\mu b+\cdots]), \tag{3.7}$$

where $\gamma=f''(\bar{a})/2$, $\gamma'=f'''(\bar{a})/6$. The convolution operation $*$ is defined by

$$w*b(\mathbf{r},\theta,t)=\int_0^\pi w(\theta-\theta')b(\mathbf{r},\theta',t)\frac{d\theta'}{\pi}, \tag{3.8}$$

whereas

$$[w_{\text{hoz}}\circ b](\mathbf{r},\theta,t)=\int w_{\text{hoz}}(\mathbf{r},\theta|\mathbf{r}',\theta')H(|\mathbf{r}-\mathbf{r}'|-d_1)$$

$$\times b(\mathbf{r}',\theta',t)\frac{d\theta'}{\pi}d\mathbf{r}' \tag{3.9}$$

and $w_{\text{hoz}}(\mathbf{r},\theta|\mathbf{r}',\theta')$ given by Eq. (2.9). Substitute into Eq. (3.7) the perturbation expansion

$$b=\varepsilon^{1/2}b_1+\varepsilon b_2+\varepsilon^{3/2}b_3+\cdots. \tag{3.10}$$

Finally, introduce a slow time scale $\tau=\varepsilon t$ and collect terms with equal powers of ε. This leads to a hierarchy of equations of the form [up to $O(\varepsilon^{3/2})$]

$$\mathcal{L}b_1=0, \tag{3.11}$$

$$\mathcal{L}b_2=v_2,$$

$$\equiv\gamma w b_1^2+\beta_0 f(\bar{a})w_{\text{hoz}}\circ 1, \tag{3.12}$$

$$\mathcal{L}b_3=v_3,$$

$$\equiv-\frac{\partial b_1}{\partial\tau}+w*[\mu_c\Delta\mu b_1+\gamma' b_1^3+2\gamma b_1 b_2],$$

$$+\mu_c\beta_0 w_{\text{hoz}}\circ b_1 \tag{3.13}$$

with the linear operator $\mathcal{L}$ defined according to

$$\mathcal{L}b=b-\mu_c w*b. \tag{3.14}$$

The first equation in the hierarchy, Eq. (3.11), has solutions of the form

$$b_1(\mathbf{r},\theta,\tau)=z(\mathbf{r},\tau)e^{2i\theta}+\bar{z}(\mathbf{r},\tau)e^{-2i\theta}. \tag{3.15}$$

We obtain a dynamical equation for the complex amplitude $z(\mathbf{r},\tau)$ by deriving solvability conditions for the higher order equations.

We proceed by taking the inner product of Eqs. (3.12) and (3.13) with the dual eigenmode $\widetilde{b}(\theta)=e^{2i\theta}$. The inner product of any two functions of θ is defined as

$$\langle u|v\rangle=\int_0^\pi u^*(\theta)v(\theta)\frac{d\theta}{\pi}. \tag{3.16}$$

With respect to this inner product, the self-adjoint linear operator $\mathcal{L}$ satisfies $\langle\widetilde{b}|\mathcal{L}b_p\rangle=\langle\mathcal{L}\widetilde{b}|b_p\rangle=0$ for all p. Since $\mathcal{L}b_p=v_p$, we obtain a hierarchy of solvability conditions $\langle\widetilde{b}|v_p\rangle=0$ for $p=2,3,\ldots$. It can be shown from Eqs. (3.9), (3.12), and (3.15) that the first solvability condition is identically satisfied. The solvability condition $\langle\widetilde{b}|v_3\rangle=0$ generates a cubic amplitude equation for $z(\mathbf{r},\tau)$. As a further simplification we set $\gamma=0$, since this does not alter the basic structure of the amplitude equation. Using Eqs. (2.9), (3.9), (3.13), and (3.15) we then find that

$$\frac{\partial z(\mathbf{r},\tau)}{\partial\tau}=z(\mathbf{r},\tau)[\Delta\mu-\Gamma|z(\mathbf{r},\tau)|^2]+\beta_0\mu_c\int_{\mathbf{R}^2}$$

$$\times[J_+(\mathbf{r}-\mathbf{r}')z(\mathbf{r}',\tau)+J_-(\mathbf{r}-\mathbf{r}')\bar{z}(\mathbf{r}',\tau)]d\mathbf{r}', \tag{3.17}$$

where $\Gamma=-3\gamma'/\mu_c$,

$$J_\pm(\mathbf{r})=\int_0^\pi\int_0^\pi e^{-2i(\theta\mp\theta')}w^\Delta(\theta-\theta')G(|\mathbf{r}|)\mathcal{P}\{\arg(\mathbf{r})$$

$$-[\theta+\theta']/2\}\frac{d\theta d\theta'}{\pi^2}, \tag{3.18}$$

and

$$G(s)=\mathcal{G}(s)H(s-d_1). \tag{3.19}$$

The kernel J_+ can be simplified by making the change of variables $\theta,\theta'\to\theta_\pm=[\theta\pm\theta']/2$ and integrating to obtain

$$J_+(\mathbf{r})=W_1^\Delta G(|\mathbf{r}|), \tag{3.20}$$

where W_1^Δ is the first Fourier coefficient of $w^\Delta(\theta)$, see Eq. (2.12). Also note that in the absence of any anisotropy ($\mathcal{P}$

$\equiv 1$), the second kernel $J_-(\mathbf{r}) \equiv 0$ so that Eq. (3.17) reduces to

$$\frac{\partial z(\mathbf{r}, \tau)}{\partial \tau} = z(\mathbf{r}, \tau)[\Delta \mu - \Gamma |z(\mathbf{r}, \tau)|^2]$$

$$+ \beta_0 \mu_c W_1^\Delta \int_{\mathbf{R}^2} G(|\mathbf{r} - \mathbf{r}'|) z(\mathbf{r}', \tau). \quad (3.21)$$

In order to extend the above analysis to the case of finite propagation speeds v, we need to assume a certain scaling rule for v, namely, $v = \varepsilon v_0$ with $v_0 = O(1)$. First note Eq. (3.7) still holds for finite propagation speeds provided that the convolution defined by Eq. (3.9) is modified by taking $b(\mathbf{r}', \theta', t) \rightarrow b(\mathbf{r}', \theta', t - |\mathbf{r}' - \mathbf{r}|/v)$. Introducing a slow time scale $\tau = \varepsilon t$ then leads to the functional form $b(\mathbf{r}', \theta', \tau - |\mathbf{r}' - \mathbf{r}|/v_0)$ provided that v has the prescribed scaling behavior. Such scaling is consistent with the slow propagation speeds of the horizontal connections. With this modification, the perturbation analysis proceeds as before, leading to the delayed nonlocal GL equation

$$\frac{\partial z(\mathbf{r}, \tau)}{\partial \tau} = z(\mathbf{r}, \tau)[\Delta \mu - \Gamma |z(\mathbf{r}, \tau)|^2]$$

$$+ \beta_0 \mu_c \int_{\mathbf{R}^2} [J_+(\mathbf{r} - \mathbf{r}') z(\mathbf{r}', \tau - |\mathbf{r} - \mathbf{r}'|/v_0)$$

$$+ J_-(\mathbf{r} - \mathbf{r}') \bar{z}(\mathbf{r}', \tau - |\mathbf{r} - \mathbf{r}'|/v_0)] d\mathbf{r}'. \quad (3.22)$$

One of the novel features of the nonlocal GL Eqs. (3.17) and (3.22) when compared to other synaptically coupled amplitude equations (see, e.g., Ref. [16]) is the presence of the linear term $\bar{z}$ in the convolutions. This term reflects the anisotropy of the horizontal connections and implies that the amplitude equation is not equivariant with respect to the phase transformation $z \rightarrow e^{i\psi} z$. The breaking of phase symmetry has important implications for the type of eigenmodes that are excited when the uniform stationary solution becomes unstable, and is a manifestation of the underlying Euclidean shift-twist symmetry of the full model (see Sec. IV).

It is important to note that, as in other pattern forming systems [2,5], the nonlocal GL amplitude equations (3.17) and (3.22) are only approximations of the full network models (2.6) and (2.16) even when they operate sufficiently close to an instability. This then raises the issue of how well solutions to the GL equations approximate solutions of the original Wilson-Cowan equations. Unfortunately, even in the case of local GL equations there are relatively few results regarding the accuracy of solutions. In spite of these limitations, amplitude equations are still useful because they provide insights into the universal behavior of systems close to points of instability, independently of the detailed structure of specific models.

IV. STABILITY ANALYSIS

The delayed nonlocal GL Eq. (3.22) has the trivial solution $z = 0$, which corresponds to the uniform stationary solution of Eq. (3.1), $a = \bar{a}$. Linearizing about this solution gives

the following linear equation for $(z, \bar{z})$ (together with the complex conjugate equation)

$$\frac{\partial z(\mathbf{r}, \tau)}{\partial \tau} = \Delta \mu z(\mathbf{r}, \tau) + \beta_0 \int [J_+(\mathbf{r} - \mathbf{r}') z(\mathbf{r}', \tau - |\mathbf{r} - \mathbf{r}'|/v_0)$$

$$+ J_-(\mathbf{r} - \mathbf{r}') \bar{z}(\mathbf{r}', \tau - |\mathbf{r} - \mathbf{r}'|/v_0)] d\mathbf{r}'. \quad (4.1)$$

where we have absorbed a factor of μ_c into β_0. Assuming a solution of the form $z(\mathbf{r}, \tau) = u(\mathbf{r}) e^{\lambda \tau} + v(\mathbf{r}) e^{\bar{\lambda} \tau}$, we obtain the pair of equations

$$\lambda u(\mathbf{r}) = \Delta \mu u(\mathbf{r}) + \beta_0 \int [J_+(\mathbf{r} - \mathbf{r}') e^{-\lambda |\mathbf{r} - \mathbf{r}'|/v_0} u(\mathbf{r}')$$

$$+ J_-(\mathbf{r} - \mathbf{r}') e^{-\lambda |\mathbf{r} - \mathbf{r}'|/v_0} \bar{v}(\mathbf{r}')] d\mathbf{r}', \quad (4.2)$$

$$\bar{\lambda} v(\mathbf{r}) = \Delta \mu v(\mathbf{r}) + \beta_0 \int [J_+(\mathbf{r} - \mathbf{r}') e^{-\bar{\lambda} |\mathbf{r} - \mathbf{r}'|/v_0} v(\mathbf{r}')$$

$$+ J_-(\mathbf{r} - \mathbf{r}') e^{-\bar{\lambda} |\mathbf{r} - \mathbf{r}'|/v_0} \bar{u}(\mathbf{r}')] d\mathbf{r}' \quad (4.3)$$

and their complex conjugates. Fourier transforming Eqs. (4.2) and (4.3) yields

$$\lambda \hat{u}(\mathbf{k}) = \Delta \mu \hat{u}(\mathbf{k}) + \beta_0 [\hat{J}_+(\mathbf{k}, \lambda) \hat{u}(\mathbf{k}) + \hat{J}_-(\mathbf{k}, \lambda) \overline{\hat{v}(-\mathbf{k})}], \quad (4.4)$$

$$\bar{\lambda} \hat{v}(\mathbf{k}) = \Delta \mu \hat{v}(\mathbf{k}) + \beta_0 [\hat{J}_+(\mathbf{k}, \bar{\lambda}) \hat{v}(\mathbf{k}) + \hat{J}_-(\mathbf{k}, \bar{\lambda}) \overline{\hat{u}(-\mathbf{k})}] d\mathbf{r}', \quad (4.5)$$

where

$$\hat{J}_\pm(\mathbf{k}, \lambda) = \int_{\mathbf{R}^2} e^{-i\mathbf{k} \cdot \mathbf{r}} J_\pm(\mathbf{r}) e^{-\lambda |\mathbf{r}|} d\mathbf{r}. \quad (4.6)$$

Substituting for $J_\pm$ using Eq. (3.18), performing the change of variables $\theta_\pm = [\theta \pm \theta']/2$ and writing $\mathbf{k} = k(\cos \varphi, \sin \varphi)$, $\mathbf{r} = r(\cos \psi, \sin \psi)$ gives

$$\hat{J}_\pm(\mathbf{k}, \lambda) = \int_0^\infty \int_0^{2\pi} d\psi r dr G(r) e^{-\lambda r} e^{-ikr \cos(\varphi - \psi)}$$

$$\times \left[\int_0^\pi \int_0^\pi e^{-4i\theta_\mp} w^\Delta(2\theta_-) \mathcal{P}(\psi - \theta_+) \frac{d\theta_+ d\theta_-}{2\pi^2} \right]. \quad (4.7)$$

Using the Bessel function expansion

$$e^{-ix \cos \phi} = \sum_{n=-\infty}^\infty (i)^n J_n(x) e^{in\phi}, \quad (4.8)$$

it follows that

$$\hat{J}_{\pm}(\mathbf{k},\lambda) = \sum_{n=-\infty}^{\infty} G_n(k,\lambda) \int_0^{2\pi} d\psi e^{2in(\psi-\varphi)}$$
$$\times \left[\int_0^\pi \int_0^\pi e^{-4i\theta_{\mp}} w^\Delta(2\theta_-) \mathcal{P}(\psi-\theta_+) \frac{d\theta_+ d\theta_-}{2\pi^2} \right],$$
(4.9)

where

$$G_n(k,\lambda) = (-1)^n \int_0^\infty r G(r) J_{2n}(kr) e^{-\lambda r} dr. \quad (4.10)$$

We can now integrate over the angles $\psi, \theta_\pm$ so that

$$\hat{J}_+(\mathbf{k},\lambda) = W_1^\Delta G_0(k,\lambda) \quad (4.11)$$

and

$$\hat{J}_-(\mathbf{k},\lambda) = e^{-4i\varphi} W_0^\Delta \mathcal{P}_2 G_2(k,\lambda), \quad (4.12)$$

with

$$\mathcal{P}_2 = \int_0^\pi e^{-4i\phi} \mathcal{P}(\phi) \frac{d\phi}{\pi} = \frac{\sin(4\eta)}{4\eta}, \quad (4.13)$$

for $\mathcal{P}$ given by Eq. (2.11). For notational convenience we set $W_n^\Delta = 1$.

Setting $U(\mathbf{k}) = e^{2i\varphi}\hat{u}(\mathbf{k})$ and $V(\mathbf{k}) = e^{2i\varphi}\hat{v}(\mathbf{k})$ in Eqs. (4.4) and (4.5) leads to the pair of equations

$$\lambda U(\mathbf{k}) = \Delta\mu U(\mathbf{k}) + \beta_0[G_0(k,\lambda)U(\mathbf{k}) + \mathcal{P}_2 G_2(k,\lambda)\overline{V(-\mathbf{k})}],$$
(4.14)

$$\bar{\lambda} V(\mathbf{k}) = \Delta\mu V(\mathbf{k}) + \beta_0[G_0(k,\bar{\lambda})V(\mathbf{k}) + \mathcal{P}_2 G_2(k,\bar{\lambda})\overline{U(-\mathbf{k})}].$$
(4.15)

Using the identity $\overline{G_n(k,\lambda)} = G_n(k,\bar{\lambda})$, we obtain the pair of solutions $\overline{V(-\mathbf{k})} = \pm U(\mathbf{k})$ with associated eigenvalues $\lambda = \lambda_\pm(k)$ obtained by solving the implicit equations

$$\lambda_\pm = \Delta\mu + \beta_0[G_0(k,\lambda_\pm) \pm \mathcal{P}_2 G_2(k,\lambda_\pm)]. \quad (4.16)$$

The corresponding eigensolutions of the linear GL Eq. (4.1) are then of the form

$$z_{\pm,\mathbf{k}}(\mathbf{r},\tau) = e^{-2i\varphi}[ce^{i\mathbf{k}\cdot\mathbf{r}}e^{\lambda_\pm(k)\tau} \pm \bar{c}e^{-i\mathbf{k}\cdot\mathbf{r}}e^{\bar{\lambda}_\pm(k)\tau}], \quad (4.17)$$

where c is a constant complex amplitude.

Substituting Eq. (4.17) into Eq. (3.15) and introducing the decomposition $\lambda_\pm = \rho_\pm + i\omega_\pm$ with $\rho_\pm, \omega_\pm$ real shows that the linear eigenmodes of the full system described by Eq. (2.16) are given by (after rescaling $c \to c/2$)

$$a_+(\mathbf{r},\theta,t) = e^{\varepsilon\rho_+ t}[ce^{i(\mathbf{k}\cdot\mathbf{r}+\varepsilon\omega_+ t)} + \bar{c}e^{-i(\mathbf{k}\cdot\mathbf{r}+\varepsilon\omega_+ t)}]\cos(2[\theta-\varphi])$$
(4.18)

and

$$a_-(\mathbf{r},\theta,t) = e^{\varepsilon\rho_- t}[ce^{i(\mathbf{k}\cdot\mathbf{r}+\varepsilon\omega_- t)} + \bar{c}e^{-i(\mathbf{k}\cdot\mathbf{r}+\varepsilon\omega_- t)}]\sin(2[\theta-\varphi]).$$
(4.19)

The even eigenmode a_+ represent a traveling $(\omega_\pm \neq 0)$ or stationary $(\omega_\pm = 0)$ plane wave $f(\mathbf{r},t) = ce^{i(\mathbf{k}\cdot\mathbf{r}+\varepsilon\omega_+ t)} + $c.c.

modulated by the factor $\cos(2[\theta-\varphi])$ with $\varphi = \arg(\mathbf{k})$ [78]. It follows that the location of the peak response with respect to orientation preference θ alternates between $\theta = \varphi$ when $f(\mathbf{r},t) > 0$ and $\theta = \varphi + \pi/2$ when $f(\mathbf{r},t) < 0$. Thus, we can represent the activity as a stripe pattern in which the peak of the orientation tuning curve alternates between these two directions. Similarly, in the case of the odd eigenmode a_-, the peak response with respect to θ alternates between $\theta = \varphi + \pi/4$ and $\theta = \varphi - \pi/4$. The existence of distinct even and odd eigenmodes (4.18) and (4.19) is a reflection of the underlying shift-twist symmetry of the full system given by Eq. (2.16) [10,11]. In the purely isotropic case $(\mathcal{P}_2 = 0)$, there is a single dispersion branch satisfying $\lambda(k) = \Delta\mu + \beta_0 G_0[k,\lambda(k)]$ and there is no longer any specific relationship between the direction of the wave vector $\mathbf{k}$ and the peaks of the orientation tuning curves, reflecting the fact that Eq. (2.16) now has $\mathbf{E}(2) \times \mathbf{O}(2)$ symmetry.

Since $G_n(k,\lambda)$, $n = 0,2$ are bounded functions [see Eq. (4.10)], it follows from Eq. (4.16) that if $\Delta\mu \ll 0$ then Re $\lambda_\pm(k) < 0$ for all k and the uniform state $z = 0$ is linearly stable. However, as $\Delta\mu$ is increased we expect a critical point to be reached where eigenmodes having a critical wave number k_c and frequency ω_c become marginally stable. Beyond this critical point these eigenmodes will start to grow leading to the formation of stationary periodic patterns ($k_c \neq 0$, $\omega_c = 0$), bulk oscillations ($k_c = 0$, $\omega_c \neq 0$) or spatiotemporal patterns ($k_c \neq 0$, $\omega_c \neq 0$). In the following we investigate which of these bifurcation scenarios occur both for zero delays and nonzero delays and show that a Turing-Hopf bifurcation does not occur.

A. Infinite propagation speeds $(v_0 \to \infty)$

In the absence of axonal propagation delays, Eq. (4.16) reduces to the simpler form

$$\lambda_\pm = \Delta\mu + \beta_0[G_0(k,0) \pm \mathcal{P}_2 G_2(k,0)]. \quad (4.20)$$

In this limiting case $\lambda_\pm(k)$ are real for all k thus precluding the possibility of a Hopf bifurcation. Setting

$$\Lambda_\pm(k) = -[G_0(k,0) \pm \mathcal{P}_2 G_2(k,0)], \quad (4.21)$$

we see from Eq. (4.20) that the condition for linear stability of the uniform state in the presence of horizontal connections reduces to

$$\Delta\mu < \beta_0 \Lambda_\pm(k)$$

for all k. Let

$$\Lambda_M = \max_{k \geq 0}\{\Lambda_+(k), \Lambda_-(k)\} \quad \text{at } k = k_M \quad (4.22)$$

and

$$\Lambda_m = \min_{k \geq 0}\{\Lambda_+(k), \Lambda_-(k)\} \quad \text{at } k = k_m. \quad (4.23)$$

Denoting the critical point by $\Delta\mu_c$, it follows that for excitatory horizontal connections $(\beta_0 > 0)$ we have $\Delta\mu_c = \varepsilon\beta_0\Lambda_m$, whereas for inhibitory horizontal connections $\Delta\mu_c = -\varepsilon|\beta_0|\Lambda_M$. It turns out that only the inhibitory case yields a pattern forming instability, that is, $k_m = 0$, $k_M > 0$. If
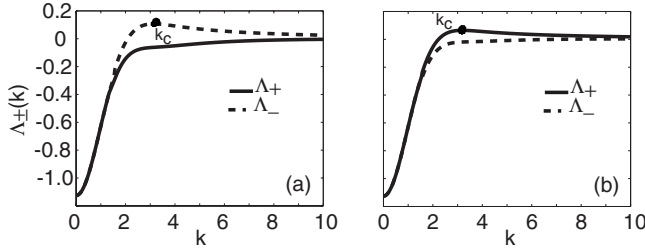
FIG. 2. (a) Plot of functions $\Lambda_+(k)$ (solid line) and $\Lambda_-(k)$ (dashed line) for $\eta = \pi/6$ (strong anisotropy). The critical wave number for spontaneous pattern formation is k_c. The marginally stable eigenmodes are odd functions of θ. Parameter values are $d_1 = 0.2$, $\beta_0 = -0.9$, $W_0^\Delta = W_1^\Delta = 1$. (b) Corresponding plots for $\eta = \pi/3$ (weak anisotropy). The marginally stable eigenmodes are now even functions of θ.

$\Lambda_+(k_M) > \Lambda_-(k_M)$ then the first eigenmodes to become excited are the even eigenmodes with wave number k_M. The infinite degeneracy arising from rotation invariance means that all modes lying on the circle $|\mathbf{k}| = k_M$ become marginally stable at the critical point [79]. Similarly, if $\Lambda_+(k_M) < \Lambda_-(k_M)$ then the first eigenmodes to become excited are the odd eigenmodes. Equation (4.12) implies that if the degree of anisotropy $\eta = \pi/4$, then $\mathcal{J}_-(k) = 0$ and there is an even/odd mode degeneracy, that is, $\Lambda_+(k) = \Lambda_-(k)$ for all k. This suggests that there is a switch from excitation of even modes to odd eigenmodes as η crosses $\pi/4$. This is illustrated in Fig. 2 where we plot $\Lambda_\pm(k)$ as a function of k for inhibitory horizontal connections ($\beta_0 < 0$).

B. Finite propagation speeds

For finite propagation speeds v_0, the eigenvalues $\lambda_\pm(k)$ are typically complex valued and Eq. (4.16) has to be solved numerically. It is now possible for a Hopf bifurcation to occur instead of a stationary bifurcation. A necessary condition

for the occurrence of a Hopf bifurcation is that $\lambda_\pm(k) = i\omega_\pm$ solves Eq. (4.16) for some k in either the even or odd case:

$$i\omega_\pm = \Delta\mu + \beta_0 \left\{ \int_0^\infty rG(r)[J_0(kr) \pm \mathcal{P}_2 J_4(kr)] e^{-i\omega_\pm r/v_0} dr \right\}.$$

$$(4.24)$$

Using Euler's formula and separating real and imaginary parts of Eq. (4.24) gives a system of two equations each for $\omega_\pm$:

$$\Delta\mu = -\beta_0 \int_0^\infty rG(r)[J_0(kr) \pm \mathcal{P}_2 J_4(kr)]\cos(\omega_\pm r/v_0) dr$$

$$\equiv C_\pm(k, \omega_\pm), \qquad (4.25)$$

$$0 = -\beta_0 \int_0^\infty rG(r)[J_0(kr) \pm \mathcal{P}_2 J_4(kr)]\sin(\omega_\pm r/v_0) dr - \omega_\pm,$$

$$\equiv S_\pm(k, \omega_\pm). \qquad (4.26)$$

In order to determine $\omega_\pm$, we generate contour plots of the functions $C_\pm(k, \omega)$ and $S_\pm(k, \omega)$ in the (k, ω) plane. We then find the minimum value $\Delta\mu_\pm$ of $\Delta\mu$ for which the contour or isocline $C_\pm(k, \omega) = \Delta\mu$ intersects the curve $S_\pm(k, \omega) = 0$. First suppose that $\Delta\mu_- < \Delta\mu_+$ and set $\Delta\mu_c = \Delta\mu_-$. The critical point (k_c, ω_c) satisfying the marginal stability condition $C_-(k_c, \omega_c) = \Delta\mu_c$ then determines the critical frequency ω_c and the critical wave number k_c for excitation of the odd eigenmodes following destabilization of the uniform state. Similarly, if $\Delta\mu_c = \Delta\mu_+ < \Delta\mu_-$ then $C_+(k_c, \omega_c) = \Delta_c$ is the marginal stability condition for excitation of the even eigenmodes.

The above construction is illustrated in Figs. 3–5 for inhibitory horizontal connections ($\beta_0 < 0$) and both fast and slow axonal delays. For sufficiently large axonal speeds v_0 and strong (weak) anisotropy, the critical contour $C_-(k, \omega)$
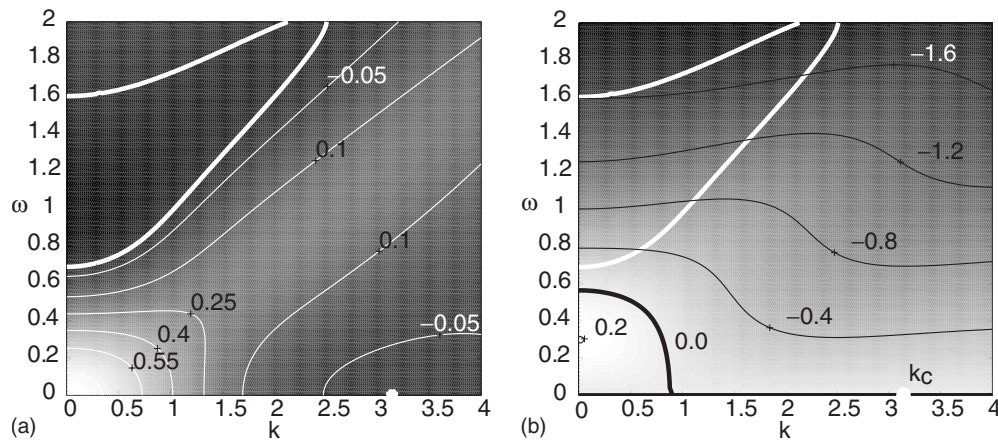

FIG. 3. Turing instability in the case of fast axonal propagation and strong anisotropy. Contour plots of (a) $C_-(k, \omega)$ and (b) $S_-(k, \omega)$ in the (k, ω) plane are generated from Eqs. (4.25) and (4.26). The critical contour $C_-(k, \omega) = \Delta\mu_c$ with $\Delta\mu_c \approx -0.07$ is highlighted in (a) and consists of the union of a continuous (thick white) curve and an isolated point on the k axis, where $C_-(k_c, 0) = \Delta\mu_c$. This contour is also shown in (b) along with the two branches of the contour $S_-(k, \omega) = 0$ (thick black curves). The point of intersection $(k, \omega) = (k_c, 0)$ gives the selected wave number of the Turing instability. Here $\beta_0 = -0.9$, $d_1 = 0.2$, $\eta = \pi/6$, $v_0 = 0.5$. (In all figures the units of time and space are fixed by setting the synaptic time constant $\tau_m = 1$ and the range of horizontal connections $\xi = 1$, respectively.)
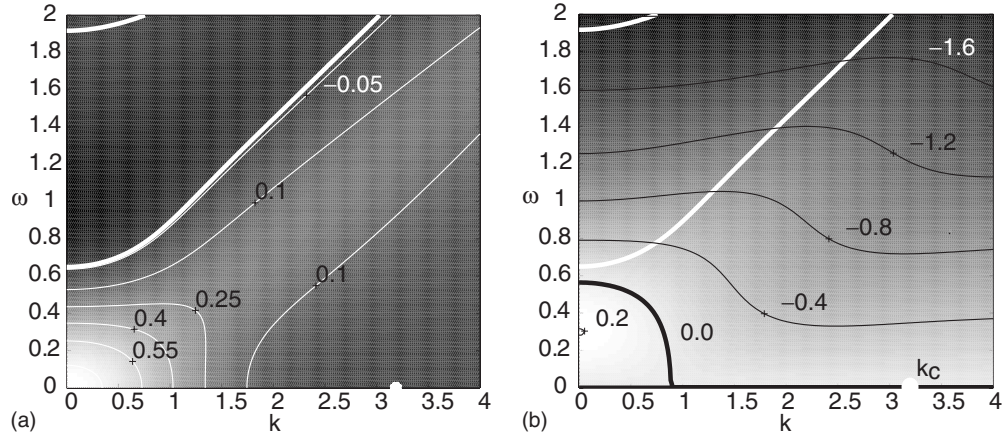
FIG. 4. Turing instability in the case of fast axonal propagation and weak anisotropy. Contour plots of (a) $C_+(k,\omega)$ and (b) $S_+(k,\omega)$ in the (k,ω) plane are generated from Eqs. (4.25) and (4.26). The critical contour $C_+(k,\omega)=\Delta\mu_c$ with $\Delta\mu_c \approx -0.04$ is highlighted in (a) and consists of the union of a continuous (thick white) curve and an isolated point on the k axis where $C_+(k_c,0)=\Delta\mu_c$. This contour is also shown in (b) along with the two branches of the contour $S_+(k,\omega)=0$ (thick black curves). The point of intersection $(k,\omega)=(k_c,0)$ gives the selected wave number of the Turing instability. Same parameter values as in Fig. 3 except $\eta=\pi/3$.

$=\Delta\mu_c$ $[C_+(k,\omega)=\Delta\mu_c]$ intersects the trivial branch of the contour $S_-(k,\omega)=0$ $[S_+(k,\omega)=0]$ at the isolated point $(k_c,0)$. This establishes that destabilization of the uniform state $z=0$ still occurs via a Turing bifurcation, resulting in the growth of odd (even) eigenmodes, see Figs. 3 and 4. On the other hand, for sufficiently small v_0, the critical contour $C_\pm(k,\omega)=\Delta\mu_\pm$ intersects the nontrivial branch of the curve $S_\pm(k,\omega)=0$ at $k=0$ with $\omega_+=\omega_-=\omega_c$ and $\Delta\mu_+=\Delta\mu_-=\Delta\mu_c$ $\neq 0$, see Fig. 5. Hence, the bifurcation point is independent of the degree of anisotropy and corresponds to a bulk Hopf instability rather than a stationary Turing instability. In Fig. 6(a) we plot the stability boundaries in $\Delta\mu$ vs v_0 parameter space for bulk oscillations, stationary patterns, and the uniform state in the case of strong anisotropy. (Similar results are obtained in the case of weak anisotropy.) All of these curves can be determined numerically from the implicit dispersion relation (4.16). In Fig. 6(b) we plot the dependence of the Hopf frequency ω on the axonal propagation speed v_0.

In our analysis we have nondimensionalized time and space by setting $\tau_m=\xi=1$, introduced a slow time scale $\tau=\varepsilon t$ and rescaled the conduction velocity according to $v=\varepsilon v_0$. Figure 6(a) implies that there is a switch between bulk oscillations and stationary patterns when $v_0 \approx 0.4$. In terms of physiological quantities, this corresponds to a conduction velocity $v=\varepsilon v_0\xi/\tau_m=0.4\varepsilon$ ms^{-1} (assuming that $\tau_m=5$ ms and $\xi=5$ mm). Since $\varepsilon \ll 1$, we see that the crossover point is smaller than the typical conduction velocity of horizontal connections, which lies in the range $0.2-0.4$ ms^{-1} [67]. This suggests that under normal physiological conditions, axonal delays are not sufficient to disrupt the spatial patterns found in our previous work [10–12]. However, our analysis predicts that bulk oscillations might arise if the horizontal connections are diseased so that their conduction velocities are significantly reduced. Figure 6(b) suggests that the resulting oscillations will be slow since the frequency is $\varepsilon\omega_c$ with
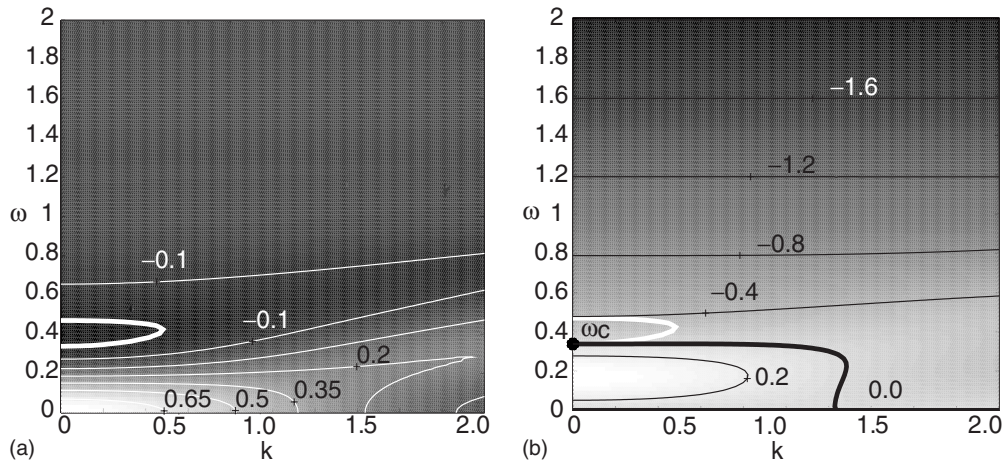

FIG. 5. Hopf instability in the case of slow axonal propagation. Same as Fig. 3 except that $v_0=0.2$. Contour plots of (a) $C_-(k,\omega)$ and (b) $S_-(k,\omega)$ in the (k,ω) plane are generated from Eqs. (4.25) and (4.26). The highlighted white curve in (a) corresponds to the critical contour $C_-(k,\omega)=\Delta\mu_c$ with $\Delta\mu_c \approx -0.22$. This curve is also shown in (b) along with the contour $S_-(k,\omega)=0$ (thick black curve). The point of intersection $(k,\omega)=(0,\omega_c)$ determines the Hopf frequency.
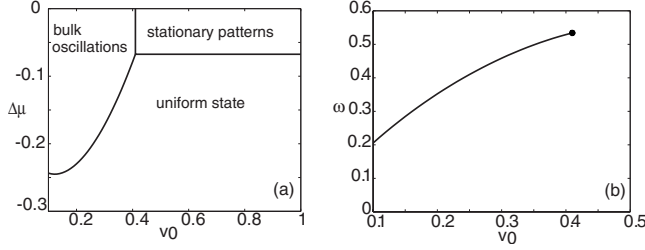
FIG. 6. (a) Stability curves in the $(\Delta\mu, v_0)$ plane. (b) Hopf frequency ω vs propagation speed v_0. Same parameter values as Fig. 3.

$\omega_c \approx 0.4$. In physiological units this corresponds to a frequency $f = \varepsilon 0.4/(2\pi\tau_m) \approx 13\varepsilon$ Hz.

C. Linear stability of roll patterns

One of the interesting features of the standard GL equation is that one can find exact spatially periodic solutions and use this to identify additional instabilities [1,2]. This is more difficult in the case of the nonlocal GL Eq. (3.22) due to the presence of the linear term $\bar{z}$ in the convolution. However, in the special case of isotropic weights [for which $J_-(\mathbf{r}) \equiv 0$], the $\bar{z}$ term disappears so that the eigenmode $z(\mathbf{r}) \equiv A e^{i\mathbf{k} \cdot \mathbf{r}}$ becomes an exact solution of the isotropic GL Eq. (3.21) for appropriate choices of the complex amplitude A. That is, by direct substitution

$$0 = \Delta\mu - |A|^2 + \beta_0 G_0(k), \qquad (4.27)$$

where we have rescaled z so that $\Gamma = 1$, absorbed a factor μ_c into β_0 and set $W_1^\Delta = 1$, $G_n(k,0) = G_n(k)$. Thus, the amplitude A is related to the wave number k according to $|A| = A(k)$ with

$$A(k) = \sqrt{\Delta\mu - |\beta_0| G_0(k)}, \qquad (4.28)$$

Positivity of $A(k)$ implies that an eigenmode of wave number k only exists if

$$G_0(k) \leq \frac{\Delta\mu}{|\beta_0|}. \qquad (4.29)$$

In order to determine the linear stability of these solutions, we set $z(\mathbf{r}, \tau) = A e^{i\mathbf{k} \cdot \mathbf{r}} + v(\mathbf{r}) e^{\sigma\tau}$ with $A = |A(k)|$ and Taylor expand Eq. (3.21) to first order in v:

$$\sigma v(\mathbf{r}) = (\Delta\mu - 2|A|^2) v(\mathbf{r}) - A^2 \bar{v}(\mathbf{r})$$
$$+ \beta_0 \int G(|\mathbf{r} - \mathbf{r}'|) v(\mathbf{r}') d\mathbf{r}'. \qquad (4.30)$$

Under the ansatz

$$v(\mathbf{r}) = e^{i\mathbf{k} \cdot \mathbf{r}}[a e^{i\mathbf{q} \cdot \mathbf{r}} + b e^{-i\mathbf{q} \cdot \mathbf{r}}], \qquad (4.31)$$

where a, b are complex amplitudes, we find

$$\sigma(a e^{i\mathbf{q} \cdot \mathbf{r}} + b e^{i\mathbf{q} \cdot \mathbf{r}}) = F(k+q) a e^{i\mathbf{q} \cdot \mathbf{r}} + F(k-q) b e^{-i\mathbf{q} \cdot \mathbf{r}}$$
$$- A^2(\bar{a} e^{-i\mathbf{q} \cdot \mathbf{r}} + \bar{b} e^{i\mathbf{q} \cdot \mathbf{r}}), \qquad (4.32)$$
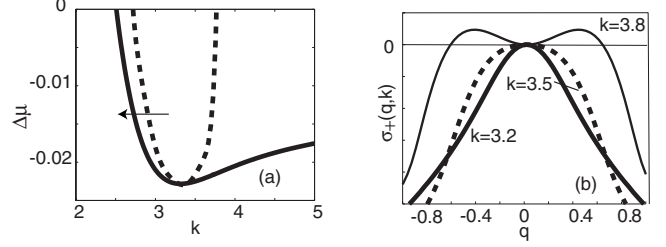
where

FIG. 7. (a) Plot of the neutral stability curve (solid) and the Eckhaus stability curve (dashed) for the isotropic nonlocal GL equation. Here $\beta_0 = -0.9$, $d_1 = 0.2$. (b) Plot of $\sigma_+(k,q)$ as a function of q for various wave numbers k and $\Delta\mu = -0.02$.

$$F(k) = \Delta\mu - 2|A|^2 + \beta_0 G_0(k) = -\Delta\mu - 2\beta_0 G_0(k). \qquad (4.33)$$

Since $e^{i\mathbf{q} \cdot \mathbf{r}}$ and $e^{-i\mathbf{q} \cdot \mathbf{r}}$ are orthogonal basis functions with respect to the L^2 inner product, we can generate an eigenvalue equation for $\Xi = (a, b, \bar{a}, \bar{b})^T$ from Eq. (4.32) and its complex conjugate, which is given by $\mathbf{M}(k)\Xi = \sigma\Xi$ and

$$\mathbf{M}(k) = \begin{pmatrix} F(k+q) & 0 & 0 & -A^2 \\ 0 & F(k-q) & -A^2 & 0 \\ 0 & -\bar{A}^2 & F(k+q) & 0 \\ -\bar{A}^2 & 0 & 0 & F(k-q) \end{pmatrix}. \qquad (4.34)$$

The resulting eigenvalues take the form

$$\sigma_\pm(q,k)$$
$$= -\Delta\mu - 2\beta_0 G_0(k) + \frac{\beta_0}{2}[G_0(k+q) + G_0(k-q)] \pm \frac{1}{2}$$
$$\times \sqrt{\beta_0^2[G_0(k+q) - G_0(k-q)]^2 + 4[\Delta\mu + \beta_0 G_0(k)]^2}. \qquad (4.35)$$

A periodic solution to the nonlocal Ginzburg-Landau equation with isotropic weights (3.21) will be stable for a given wave number k if $\text{Re}[\sigma_+(k,q)] \leq 0$ for all q.

In Fig. 7(a) we plot the marginal stability and Eckhaus stability curves for $G(s)$ given by the Gaussian (2.10). For a given $\Delta\mu$, all eigenmodes with wave numbers lying within the interior of the marginal stability curve exist according to the inequality (4.29), but only those lying within the interior of the Eckhaus stability curve are linearly stable. The corresponding dispersion curves $\sigma_+(q,k)$ for $\Delta\mu = -0.3$ and various wave numbers k are plotted as a function of q in Fig. 7(b). It can be seen that as k decreases in the direction of the arrow shown in (a), the dispersion curve crosses zero such that a band of q modes are excited, signaling an Eckhaus instability of the corresponding roll pattern. A numerical simulation illustrating the dynamics of the Eckhaus instability is shown in Fig. 8.

V. DISCUSSION

In this paper we have shown how a two-dimensional continuum model of V1, in which cells signal both the position
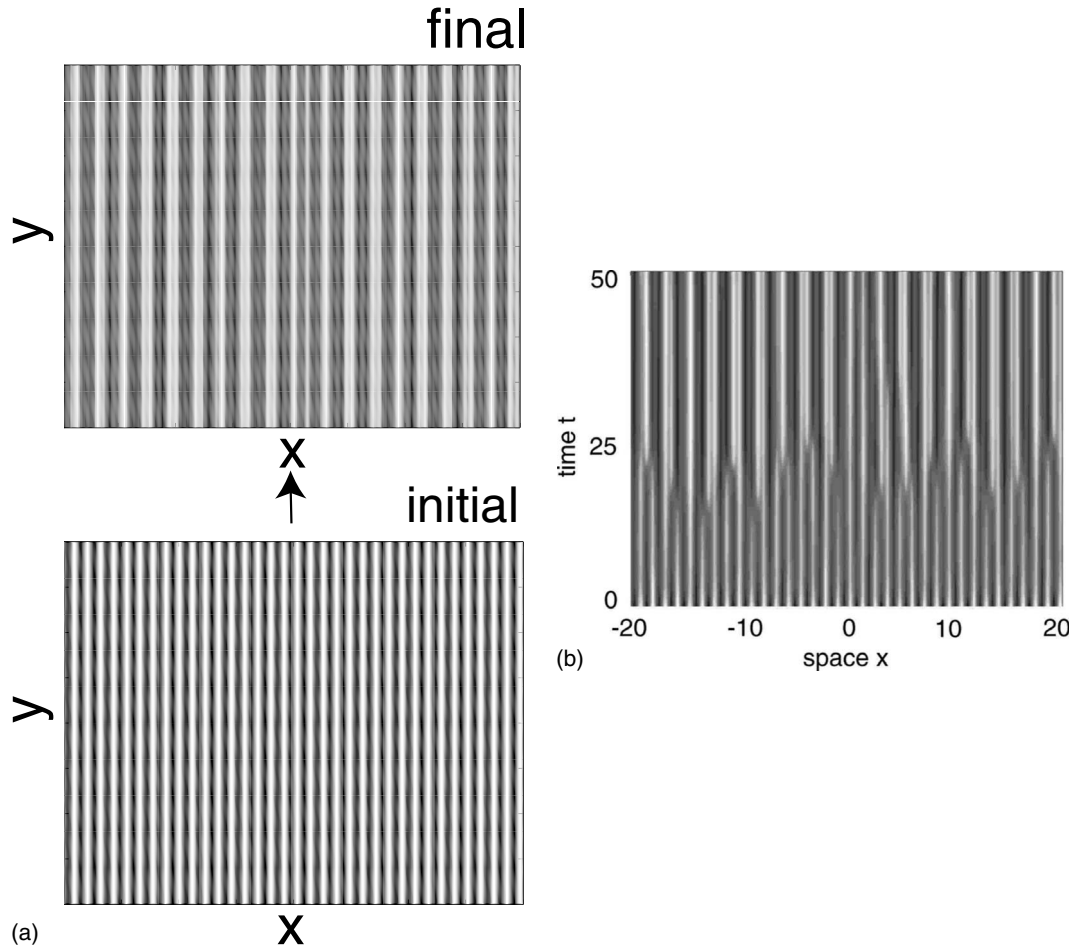
FIG. 8. Evolution of a roll pattern undergoing an Eckhaus instability. A one-dimensional transverse slice of a two-dimensional roll pattern Re $z(\mathbf{r})$ is plotted as a function of time. The initial pattern has a wave number $k=5.5$, which lies between the Eckhaus and marginal stability curves shown in Fig. 7(a) for $\Delta\mu=0$. The final stable pattern has a smaller wave number, $k=2.98$, which is located within the interior of the Eckhaus stability curve.

and orientation of a local visual stimulus, can be reduced to a nonlocal GL equation that describes spatial correlations in the complex amplitude of orientation tuning curves across cortex. For sufficiently fast horizontal connections, the nonlocal GL equation exhibits a Turing-like instability leading to the formation of stationary, spatially periodic patterns. In contrast to previous work [10,77], the pattern forming instability is generated by inhibitory long-range connections with a gap at the origin rather than by local connections described by a Mexican hat function. For sufficiently slow horizontal connections, however, the dominant instability involves a Hopf bifurcation leading to the formation of bulk oscillations rather than stationary patterns. Our analysis suggests that under normal physiological conditions, axonal propagation delays are not sufficient to disrupt the formation of spatial patterns. However, bulk oscillations could arise if the conduction velocities of the horizontal connections were significantly reduced due to some pathology.

Note that axonal delays are not the only mechanism for generating oscillations in large-scale continuum models of cortex. For example, symmetric bifurcation theory has been used to show that in the isotropic case ($\eta=\pi/2$) without delays the full system (2.6) belongs to a class of models that

generically exhibit rotating wave solutions [80]. These solutions arise from a codimension-1 steady-state bifurcation and persist under conditions of weak anisotropy. It is particularly unusual for a codimension-1 steady-state bifurcation to generate time-periodic states, and is a consequence of the additional continuous O(2) symmetry that is present in the isotropic case. Oscillations in the absence of delays can also occur via a Hopf bifurcation in a two-population model for which excitatory and inhibitory neurons form distinct pools [81]. In the case of a two-population version of Eqs. (2.6) and (2.7), the oscillations are generated by the local circuitry and lead to local standing or traveling waves with respect to the θ coordinate. These are then modulated by the long-range horizontal connections [14].

One interesting extension of our work would be to use weakly nonlinear analysis and perturbation theory to analyze the selection and stability of patterns generated by the nonlocal GL equation. For example, beyond the bifurcation point for Turing pattern formation, all eigenmodes having wave vectors lying in a continuous band around the critical circle $|\mathbf{k}|=k_c$ are excited. In classical theories of pattern formation in reaction-diffusion systems, this band of eigenmodes can be taken into account by carrying out a multiple-scale expan-

sion in space as well as time [1–4]. The resulting amplitude equation incorporates the diffusive effects of long-wavelength phase modulations of the primary pattern, including secondary instabilities away from the bifurcation point and the formation of pattern defects. In previous work, we have carried out such an analysis for a simpler one-dimensional neural model [50].

Another important extension of our work would be to include the effects of noise. This is particularly relevant due to the fact that our derivation of the nonlocal GL equation is based on the assumption that the local network is in a balanced state such that it operates close to a point of instability. A balanced state can be particularly sensitive to noise-induced fluctuations. There are two basic approaches to introducing noise into our model. One is to phenomenologically add a space-dependent additive noise term to the right-hand side of Eq. (2.6), and then to carry out a stochastic center manifold reduction along the lines of Hutt *et al.* [82]. The other is to start off with a more spatially fine-grained network model involving conductance-based integrate-and-fire point neurons, and then to derive a kinetic theory that captures the statistical dynamics of neuronal populations within coarse-grained patches [64,83]. We hope to explore both approaches in future work.

Finally, in addition to giving a universal description of spontaneous cortical dynamics sufficiently close to the point of instability, the nonlocal GL Eqs. (3.17) and (3.22) provide a framework for studying how long-range connections modulate the effects of external stimuli, under the additional assumption that the external stimuli are sufficiently weak. More specifically, suppose a compact cortical domain $U \subset \mathbf{R}^2$

is driven by an external visual stimulus and that only driven cells are sitting close to bifurcation, whereas nondriven cells are quiescent. (In fact, nondriven cells could still be spontaneously active and thus provide a source of external noise.) We can then incorporate the effect of such a drive by adding an external input to the right-hand side of Eq. (2.6) of the form $h(\mathbf{r}, \theta) = A(\mathbf{r}) e^{2i[\theta - \varphi(\mathbf{r})]} + \text{c.c.}$, and restricting spatial integration from $\mathbf{R}^2$ to U. Here the real amplitude $A(\mathbf{r})$ represents the contrast of a local stimulus and $\varphi(\mathbf{r})$ is its orientation. Note that the filtered input to a cortical cell of orientation preference θ [see Eq. (2.5)] is taken to depend on the difference in orientations $\theta - \varphi(\mathbf{r})$. Assuming that the amplitude of the stimulus scales as $A = \varepsilon^{3/2} A_0$ with $A_0 = O(1)$, we can carry out the perturbation analysis of Sec. IIIA to derive a modified GL equation of the form (for zero axonal delays)

$$\frac{\partial z(\mathbf{r}, \tau)}{\partial \tau} = z(\mathbf{r}, \tau)[\Delta\mu(\mathbf{r}) - \Gamma|z(\mathbf{r}, \tau)|^2]$$

$$+ \beta_0 \mu_c \int_U [J_+(\mathbf{r} - \mathbf{r}')z(\mathbf{r}', \tau)$$

$$+ J_-(\mathbf{r} - \mathbf{r}')\overline{z}(\mathbf{r}', \tau)]d\mathbf{r}' + A_0(\mathbf{r})e^{-2i\varphi(\mathbf{r})},$$

where variations in the contrast of the stimulus could also lead to a space-dependent bifurcation parameter $\Delta\mu(\mathbf{r})$. The above equation is a continuum version of an amplitude equation previously derived for a spatially discrete model of coupled V1 hypercolumns [13]. The continuum model is particularly useful for studying the role of long-range connections in the processing of smooth contours [84].

---

[1] M. C. Cross and P. C. Hohenberg, Rev. Mod. Phys. **65**, 851 (1993).

[2] R. Hoyle, *Pattern Formation: An Introduction to Methods.* (Cambridge University Press, Cambridge 2006).

[3] A. C. Newell and J. A. Whitehead, J. Fluid Mech. **38**, 279 (1969).

[4] L. A. Segel, J. Fluid Mech. **38**, 203 (1969).

[5] Y. Nishiura, *Far-from Equilibrium Dynamics* (American Mathematical Society, Providence, RI , 2002).

[6] Y. Kuramoto, *Chemical Oscillations, Waves and Turbulence* (Springer, New York, 1984).

[7] D. Tanaka and Y. Kuramoto, Phys. Rev. E **68**, 026219 (2003).

[8] Y. Kuramoto, Prog. Theor. Phys. **94**, 321 (1995).

[9] Y. Kuramoto and H. Nakao, Physica D **103**, 294 (1997).

[10] P. C. Bressloff, J. D. Cowan, M. Golubitsky, P. J. Thomas, and M. Wiener, Philos. Trans. R. Soc. London, Ser. B **356**, 299 (2001).

[11] P. C. Bressloff, J. D. Cowan, M. Golubitsky, and P. J. Thomas, Nonlinearity **14**, 739 (2001).

[12] P. C. Bressloff, J. D. Cowan, M. Golubitsky, P. J. Thomas, and M. Wiener, Neural Comput. **14**, 473 (2002).

[13] P. C. Bressloff and J. D. Cowan, Neural Comput. **14**, 493 (2002).

[14] P. C. Bressloff and J. D. Cowan, in *Nonlinear Dynamics:* *Where do We Go From Here?*, edited by S. J. Hogan, A. Champneys, and B. Krauskopf (Institute of Physics, Bristol, 2002), Chap. 11.

[15] D. G. Aronson, G. B. Ermentrout, and N. Kopell, Physica D **41**, 403 (1990).

[16] F. H. Hoppensteadt and E. M. Izhikevich, *Weakly Connected Neural Networks* (Springer-Verlag, New York, 1997).

[17] J. D. Drover and G. B. Ermentrout, SIAM J. Appl. Math. **63**, 1627 (2003).

[18] S. LeVay and S. B. Nelson, in *The Neural Basis of Visual Function*, edited by A. G. Leventhal (CRC Press, Boca Raton, 1991), pp. 266–315.

[19] N. V. Swindale, Network Comput. Neural Syst. **7**, 161 (1996).

[20] D. H. Hubel and T. N. Wiesel, J. Comp. Neurol. **158**, 267 (1974).

[21] The cortex is, of course, three dimensional, since it has nonzero thickness with a distinctive layered structure. However, one finds that cells with similar feature preferences tend to arrange themselves in vertical columns so that to a first approximation the layered structure of cortex can be ignored. However, it is important to note that there can be functional differences between neurons in distinct layers within the same column so that certain care has to be taken in ignoring the third dimension [26]. Given that optical imaging studies measure

the response properties of superficial layers of cortex, we consider a model based on the structure of these layers.

[22] G. G. Blasdel and G. Salama, Nature (London) **321**, 579 (1986).

[23] G. G. Blasdel, J. Neurosci. **12**, 3139 (1992).

[24] T. Bonhoeffer, D. S. Kim, D. Malonek, D. Shoham, and A. Grinvald, Eur. J. Neurosci. **7**, 1973 (1995).

[25] D. H. Hubel and T. N. Wiesel, J. Comp. Neurol. **158**, 295 (1974).

[26] J. S. Lund, A. Angelucci, and P. C. Bressloff, Cereb. Cortex **13**, 15 (2003).

[27] R. Douglas, C. Koch, M. Mahowald, K. Martin, and H. Suarez, Science **269**, 981 (1995).

[28] J. Marino, J. Schummers, D. C. Lyon, L. Schwabe, O. Beck, P. Wiesing, K. Obermayer, and M. Sur, Nat. Neurosci. **8**, 194 (2005).

[29] R. Ben-Yishai, R. Lev Bar-Or, and H. Sompolinsky, Proc. Natl. Acad. Sci. U.S.A. **92**, 3844 (1995).

[30] D. C. Somers, S. Nelson, and M. Sur, J. Neurosci. **15**, 5448 (1995).

[31] K. S. Rockland and J. Lund, J. Comp. Neurol. **216**, 303 (1983).

[32] C. D. Gilbert and T. N. Wiesel, J. Neurosci. **3**, 1116 (1983).

[33] R. Malach, Y. Amir, M. Harel, and A. Grinvald, Proc. Natl. Acad. Sci. U.S.A. **90**, 10469 (1993).

[34] T. Yoshioka, G. G. Blasdel, J. B. Levitt, and J. S. Lund, Cereb. Cortex **6**, 297 (1996).

[35] W. H. Bosking, Y. Zhang, B. Schofield, and D. Fitzpatrick, J. Neurosci. **17**, 2112 (1997).

[36] L. C. Sincich and G. G. Blasdel, J. Neurosci. **21**, 4416 (2001).

[37] A. Angelucci, J. B. Levitt, E. J. S. Walton, J.-M. Hupé, J. Bullier, and J. S. Lund, J. Neurosci. **22**, 8633 (2002).

[38] A. Angelucci and P. C. Bressloff, Prog. Brain Res. **154**, 93 (2006).

[39] A. Shmuel, M. Korman, M. Harel, S. Ullman, R. Malach, and A. Grinvald, J. Neurosci. **25**, 2117 (2005).

[40] J. D. Hirsch and C. D. Gilbert, J. Physiol. (London) **160**, 106 (1991).

[41] L. J. Toth, S. C. Rao, D. S. Kim, D. C. Somers, and M. Sur, Proc. Natl. Acad. Sci. U.S.A. **93**, 9869 (1996).

[42] C. D. Gilbert, A. Das, M. Ito, M. Kapadia, and G. Westheimer, Proc. Natl. Acad. Sci. U.S.A. **93**, 615 (1996).

[43] D. Fitzpatrick, Curr. Opin. Neurobiol. **10**, 438 (2000).

[44] J. Bullier, J. M. Hupé, A. J. James, and P. Girard, Prog. Brain Res. **134**, 193 (2001).

[45] H. R. Wilson and J. D. Cowan, Biophys. J. **12**, 1 (1972).

[46] H. R. Wilson and J. D. Cowan, Kybernetik **13**, 55 (1973).

[47] G. B. Ermentrout, Rep. Prog. Phys. **61**, 353 (1998).

[48] S. Coombes, Biol. Cybern. **93**, 91 (2005).

[49] P. C. Bressloff, Phys. Rev. Lett. **89**, 088101 (2002).

[50] P. C. Bressloff, Physica D **185**, 131 (2003).

[51] L. Schwabe, K. Obermayer, A. Angelucci, and P. C. Bressloff, J. Neurosci. **26**, 9117 (2006).

[52] D. J. Wielaard, M. J. Shelley, D. W. McLaughlin, and R. Shapley, J. Neurosci. **21**, 5203 (2001).

[53] R. B. Tootell, M. S. Silverman, E. Switkes, and R. L. De-Valois, Science **218**, 902 (1982).

[54] E. Schwartz, Biol. Cybern. **25**, 181 (1977).

[55] G. G. Blasdel and D. Campbell, J. Neurosci. **21**, 8286 (2001).

[56] H. Yu, B. J. Farley, D. Z. Jin, and M. Sur, Neuron **47**, 267 (2005).

[57] T. I. Baker and N. P. Issa, J. Neurophysiol. **94**, 775 (2005).

[58] A. Basole, L. E. White, and D. Fitzpatrick, Nature (London) **423**, 986 (2003).

[59] A similar decomposition was previously carried out in continuum versions of the coupled hypercolumn model [10–12], except that $d_0, d_1 \rightarrow 0$ and, hence, the local part reduced to $w(\theta - \theta')\delta(\mathbf{r} - \mathbf{r}')$ and the long-range connections did not have a gap.

[60] P. E. Maldonado, I. Godecke, C. M. Gray, and T. Bonhoeffer, Science **276**, 1551 (1997).

[61] J. Schummers, J. Marino, and M. Sur, Neuron **36**, 969 (2002).

[62] I. Nauhaus, A. Benucci, M. Carandini, and D. L. Ringach, Neuron **57**, 673 (2008).

[63] D. Mclaughlin, R. Shapley, M. Shelley, and D. J. Wielaard, Proc. Natl. Acad. Sci. U.S.A. **97**, 8087 (2000).

[64] D. Cai, L. Tao, M. Shelley, and D. W. Mclaughlin, Proc. Natl. Acad. Sci. U.S.A. **101**, 7757 (2004).

[65] P. C. Bressloff and J. D. Cowan, Philos. Trans. R. Soc. London **358**, 1643 (2003).

[66] G. Singh, F. Memoli, T. Ishkhanov, G. Sapiro, G. Carlsson, and D. L. Ringach, J. Vision **8**, 1 (2008).

[67] P. Girard, J. M. Hupé, and J. Bullier, J. Neurophysiol. **85**, 1328 (2001).

[68] J. J. Wright and D. T. J. Liley, Biol. Cybern. **72**, 347 (1995).

[69] V. K. Jirsa and H. Haken, Physica D **99**, 503 (1997).

[70] P. C. Bressloff and S. Coombes, Int. J. Mod. Phys. B **11**, 2343 (1997).

[71] D. Golomb and G. B. Ermentrout, Network Comput. Neural Syst. **11**, 221 (2000).

[72] P. A. Robinson, P. N. Loxley, S. C. O'Connor, and C. J. Rennie, Phys. Rev. E **63**, 041909 (2001).

[73] S. Coombes, G. J. Lord and M. R. Owen, Physica D **178**, 219 (2003).

[74] A. Hutt, M. Bestehorn, and T. Wennekers, Network Comput. Neural Syst. **14**, 351 (2003).

[75] F. M. Atay and A. Hutt, SIAM J. Appl. Math. **65**, 644 (2005).

[76] N. A. Venkov, S. Coombes, and P. C. Matthews, Physica D **232**, 1 (2007).

[77] G. B. Ermentrout and J. D. Cowan, SIAM J. Appl. Math. **34**, 137 (1979).

[78] The dispersion relation (4.20) with $\lambda_\pm = \rho_\pm + i\omega_\pm$ is in fact symmetric with respect to the transformation $\omega_\pm \rightarrow \pm \omega_\pm$ so that standing waves could also occur.

[79] One way to handle this infinite degeneracy is to restrict the space of solutions to that of doubly periodic functions corresponding to regular tilings of the plane [1,2]. The original Euclidean symmetry group is then restricted to the symmetry group of the underlying lattice. In particular, there are only a finite number of rotations and reflections to consider for each lattice (modulo an arbitrary rotation of the whole plane), which correspond to the so-called holohedries of the plane. Consequently the corresponding space of marginally stable modes is now finite-dimensional—we can only rotate eigenfunctions through a finite set of angles (for example, multiples of $\pi/2$ for a square lattice and multiples of $\pi/3$ for an hexagonal lattice). The linear eigenmodes now consist of a finite linear combination of either even $(+)$ or odd $(-)$ stationary plane waves $z(\mathbf{r}) = \sum_{n=1}^{N} e^{-2i\varphi_n}[c_n e^{i\mathbf{k}_n \cdot \mathbf{r}} \pm \bar{c}_n e^{-i\mathbf{k}_n \cdot \mathbf{r}}]$. Here $N=2$ for a square or rhombic lattice and $N=3$ for an hexagonal lattice.

Also $\mathbf{k}_1 \cdot \mathbf{k}_2 = k_c^2 \cos \varphi$ with $\varphi = \pi/2$ for $N=2$, and $\varphi = 2\pi/3$ for $N=3$ with $\mathbf{k}_3 = -\mathbf{k}_1 - \mathbf{k}_2$. Note that perturbation methods can be used to derive amplitude equations for the coefficients c_n, although the basic structure of these equations can be deduced using symmetry arguments [10,11].

[80] M. Golubitsky, L. J. Shiau, and A. Török, SIAM J. Appl. Dyn. Syst. **2**, 97 (2003).

[81] G. B. Ermentrout and J. D. Cowan, J. Math. Biol. **7**, 265 (1979).

[82] A. Hutt, A. Longtin and L. Schimansky-Geier, Physica D **237**, 755 (2008).

[83] D. Cai, L. Tao, A. A. Rangan, and D. W. Mclaughlin, Commun. Math. Sci. **4**, 97 (2006).

[84] P. R. Roelfsema, Annu. Rev. Neurosci. **29**, 203 (2006).